# Concentration, temporal variation and sources of black carbon in the Mount Everest region retrieved by real-time observation and simulation

Xintong Chen [1, 4], Shichang Kang [1, 2, 4], Zhiyuan Cong [2, 3], Junhua Yang [1], Yaoming Ma [3]

[1]State Key Laboratory of Cryospheric Science, Northwest Institute of Eco-Environment and Resources, Chinese Academy of Sciences, Lanzhou 730000, China

[2]CAS Center for Excellence in Tibetan Plateau Earth Sciences, Chinese Academy of Sciences, Beijing 100101, China

[3]Key Laboratory of Tibetan Environment Changes and Land Surface Processes, Institute of Tibetan Plateau Research, Chinese Academy of Sciences, Beijing 100101, China

[4]University of Chinese Academy of Sciences, Beijing 100049, China

*Correspondence to*: Shichang Kang (shichang.kang@lzb.ac.cn)

**Abstract.** Based on the high-resolution measurement of black carbon (BC) at Qomolangma (Mt. Everest) Station (QOMS, 28.36°N, 86.95°E, 4276 m a.s.l.) from 15 May 2015 to 31 May 2017, we investigated the seasonal and diurnal variations in BC and its potential source regions. Both monthly and daily mean BC concentrations reached the highest values in the pre-monsoon season and the lowest values in the monsoon season. The highest monthly and daily mean BC concentrations were at least one order of magnitude higher than the lowest concentrations. For the diurnal variation, the BC concentrations remained significantly high from late night to morning in the pre-monsoon season. Meanwhile, the westerly winds prevailed during this period, implying the potential for pollutants to be transported across the Himalayas from long-distance sources to QOMS along the valley. In the monsoon season, the BC concentrations remained low but peaked in the morning and in the noon, which might be caused by local emissions from cooking. By analyzing the simulation results from the backward trajectories of air masses and the fire spot distribution from the MODIS data, we found that the seasonal cycle of BC was significantly influenced by the atmospheric circulation and combustion intensity in the Mt. Everest region. The transport mechanisms of BC were further revealed using a WRF-Chem simulation during severe pollution episodes. For the pollution event in the monsoon season, BC aerosols in South Asia were uplifted and transported to the Mt. Everest region by the southerly winds in the upper atmosphere. However, for the events in the pre-monsoon season, BC from northern India was transported and concentrated on the southern slope of the Himalayas by the northwesterly winds in the lower atmosphere and then transported across the Himalayas by the mountain-valley wind. Relatively less BC from northwestern India and Central Asia was transported to the Mt. Everest region by the westerly winds in the upper atmosphere.

## 1 Introduction

Black Carbon (BC), mainly from the incomplete combustion of fossil fuels or biomass, has drawn much attention due to its influences on the environment and human health (Bond, 2004; Ramanathan et al., 2005; Anenberg et al., 2012) and is seen as an important factor that may lead to global warming, in addition to greenhouse gases (Hansen et al., 2000; Jacobson, 2002;

32  Bond et al., 2013; Ramanathan and Carmichael, 2008). BC can substantially absorb solar radiation and causes atmospheric

33  heating (Jacobson, 2001; Ramanathan et al., 2005; Ji et al., 2015). Moreover, BC can be suspended as fine particles in the

34  atmosphere for approximately one week, be transported far away from its emission sources, and then be removed by dry and

35  wet deposition (Oshima et al., 2012; Cooke et al., 2002; Jurado et al., 2008). When BC is deposited on snow and ice, it can

36  significantly reduce surface albedo (Flanner et al., 2007; He et al., 2017) and accelerate glacier and snow cover melting,

37  causing an impact on the regional climate, hydrology, and water resources (Li et al., 2018; Ming et al., 2008; Ramanathan and

38  Carmichael, 2008).

39      The Tibetan Plateau (TP), generally known as the "Third Pole", is the highest plateau with a large number of glaciers and

40  snow cover (Kang et al., 2010; Lu et al., 2010; Yao et al., 2012). Even though the TP is a remote region with few affects from

41  anthropogenic activities, previous observations have indicated that BC is an important contributor to the rapid shrinking of

42  glaciers over the TP via decreasing surface albedo and atmospheric warming (Xu et al., 2009; Yang et al., 2015; Li et al., 2017b;

43  Zhang et al., 2017b; Qu et al., 2014; Ji, 2016; Xu et al., 2016; Lee et al., 2017). Moreover, previous studies have also suggested

44  that the emissions from South Asia and East Asia are the major sources of BC on the TP (Li et al., 2016a; Lu et al., 2012; He

45  et al., 2014b; Zhang et al., 2015; Yang et al., 2018), and the high emissions from South Asia can be transported across the

46  Himalayas and further to the inland TP (Luthi et al., 2015; Xu et al., 2014; Cong et al., 2015a; Kang et al., 2016; Wan et al.,

47  2015). Meanwhile, the seasonality of BC aerosols is closely related to atmospheric circulation that helps to bring the BC

48  aerosols across the Himalayas (Cong et al., 2015a; Cong et al., 2015b; Yang et al., 2018). Additionally, a large number of

49  studies have demonstrated that the BC and dust from Central Asia and northern Africa could also be transported to the TP

50  (Wang et al., 2016; Lu et al., 2012; Zhao et al., 2012; Wu et al., 2010; Zhang et al., 2015).

51      Mt. Everest could be regarded as a very sensitive area under the influence of BC aerosols. Previous research on

52  atmospheric BC in the Mt. Everest region was mainly based on the thermal/optical analytical method, using quartz filter

53  samples (Cong et al., 2015a). However, there is still a lack of investigations on the diurnal and seasonal variations in BC in

54  this region. Therefore, to fill such gaps and understand the variations in and sources of BC in the pristine region, there is a

55  need for an efficient approach and additional studies. The Aethalometer can provide real-time high-resolution observation data

56  on the BC concentration, which is very important and necessary to better depict the characteristics of BC and its effects on the

57  environmental change.

58      In comparison with the observations, numerical models can better represent the atmospheric physical and chemical

59  processes. Many studies have used global climate models (GCMs) and chemical transport models (CTMs) to investigate the

60  origin and transportation of BC over the TP (Lu et al., 2012; Zhang et al., 2015; Menon et al., 2010; Kopacz et al., 2011; He

61  et al., 2014a). However, due to the coarse resolution, it is difficult for the CTMs and GCMs to capture the surface details of

62  the TP (Ji et al., 2015; Gao et al., 2008). Regional climate models (RCMs) can compensate for the shortcomings of coarser

63  global model grids by high-resolution simulations. In recent decades, RCMs have been developed to include multiple modules

64 and atmospheric chemistry processes. In addition, the advanced regional climate-chemistry model, Weather Research and

65 Forecasting (WRF) model (Skamarock et al., 2005) coupled with chemistry (WRF-Chem) has been successfully applied for

66 air quality research on the TP (Yang et al., 2017; Yang et al., 2018).

67     Here, we present real-time data of the BC concentration measured by the new Aethalometer model AE-33 from 15 May

68 2015 to 31 May 2017. The observed results are used to characterize the temporal variation and provide important information

69 on the possible sources and transport mechanisms of BC. By combining high-resolution measurements of the BC concentration

70 and the WRF-Chem model, we investigated the concentration level, temporal variation, and sources of BC in the Mt. Everest

71 region. The purpose of this study is to understand the impact of trans-boundary atmospheric BC on the Mt. Everest region and

72 depict the transport pathways of BC at different spatiotemporal scales.

73 **2 Materials and methods**

74 **2.1 Sampling site and meteorological conditions**

75     Mt. Everest (27.98°N, 86.92°E, 8844 m a.s.l.), the summit of the world, is located in the central Himalayas. The southern

76 slope of Mt. Everest is adjacent to the Indian continent, and the climate is warm and humid under the influence of the Indian

77 summer monsoon. Conversely, the northern side is cold and dry since the warm and humid airflow cannot reach it.

78 Qomolangma (Mt. Everest) Station for Atmospheric and Environmental Observation and Research, Chinese Academy of

79 Sciences (QOMS, 28.36°N, 86.95°E, 4276 m a.s.l.) (Fig. 1) is located on the northern slope of Mt. Everest, which was

80 established for continuous monitoring of the atmospheric environment (Cong et al., 2015a; Ma et al., 2011).

81     The meteorological parameters, i.e., air temperature, air pressure, humidity, wind speeds and wind direction, were

82 recorded by an automatic weather station at QOMS with 10 min time intervals. Meanwhile, the precipitation data were

83 collected by artificial measurement, as shown in Fig. S1. The entire year was divided into four seasons according to the Indian

84 monsoon transition characteristics, which includes pre-monsoon (March to May), monsoon (June to September), post-

85 monsoon (October to November), and winter (December to February) (Praveen et al., 2012; Zhang et al., 2017a). A clear

86 seasonal cycle of temperature and humidity can be observed in Fig. S1. Specifically, the temperature was high during the

87 monsoon season and low during winter, with a maximum in July and a minimum in January. Humidity followed a similar trend,

88 with high values from late July to early August and low values from December to February. During the observation period, the

89 wind speed increased significantly from November to April. The wind direction at QOMS is affected by the local topography,

90 which consists of a series of small valleys. During the pre-monsoon season (dry period), the westerly and southerly winds

91 begin to develop and play an important role in atmospheric pollution circulation. However, during the monsoon season, the

92 southwesterly winds prevail and bring much moisture from the Indian Ocean to the Mt. Everest region, increasing the humidity

93 and precipitation. With the retreat of the monsoon, the southwesterly winds decrease and the prevailing wind direction changes

94  to westerly and northeasterly in winter with limited moisture (Fig. S1).

95  **2.2 BC measurements**

96      There are several available methods capable of measuring BC concentrations, and these methods can be classified into

97  three categories. First is the thermal/optical method, which uses a quartz filter to collect aerosols, and they are thermally

98  volatilized in several temperature steps (Schauer et al., 2003). The signals of evolving carbon measured by thermal/optical

99  transmission (TOT) or thermal/optical reflectance (TOR) can be converted to the concentration of BC (Chow et al., 1993;

100  Chow et al., 2001). However, the time difference between sampling and detection, the impact of mineral dust, and the

101  determination of the split between organic carbon (OC) and elemental carbon (EC, the same as BC) can cause deviations (Li

102  et al., 2017a; Schauer et al., 2003). The second category is the technique of the single particle soot photometer (SP2), which

103  can quantify BC by laser-induced incandescence because BC is the predominant refractory absorbing aerosol, which can be

104  heated by an intense laser beam and emit significant thermal radiation (Stephens et al., 2003). This method measures the mass

105  of BC in individual particles, but the accuracy depends on the selected calibration material (Schwarz et al., 2010; Laborde et

106  al., 2012). Finally, the optical method measures the reduction in light intensity induced by BC aerosols collected on the

107  sampling medium (Hansen et al., 1984; Petzold and Schonlinner, 2004). The Aethalometer is a widely used instrument based

108  on the optical method that can provide real-time BC concentration measurements, but all filter-based optical methods exhibit

109  loading effects that can lead to the underestimation of BC concentrations (Bond et al., 1999; Virkkula et al., 2007; Park et al.,

110  2010; Hyvarinen et al., 2013; Drinovec et al., 2015). However, the newly developed Aethalometer model AE-33 uses a real-

111  time loading effect compensation algorithm that can provide high-quality data, which is very helpful for the accurate

112  determination of BC concentrations and source apportionment (Drinovec et al., 2015).

113      Therefore, the airborne BC concentrations at QOMS were monitored by the new Aethalometer model AE-33 (Magee

114  Scientific Corporation, USA). The instrument was set in an indoor room with an inlet installed at approximately 3 m above

115  the ground level and was operated at an airflow rate of 4 LPM with a 1 min time resolution. AE-33 has seven fixed wavelengths

116  (i.e., 370, 470, 520, 590, 660, 880 and 950 nm), which can acquire the BC concentration according to the light absorption and

117  attenuation characteristics from the different wavelengths (Hansen et al., 1984; Drinovec et al., 2015). Generally, the BC

118  concentration measured at 880 nm is used as the actual BC concentration in the atmosphere, as the absorption of other species

119  of aerosols is greatly reduced in this wavelength (Sandradewi et al., 2008a; Sandradewi et al., 2008b; Fialho et al., 2005; Yang

120  et al., 2009; Drinovec et al., 2015). Compared to previous Aethalometer models, AE-33 uses dual-spot measurement and a

121  real-time calculation of the "loading compensation parameter", which can compensate for the "spot loading effect" and obtain

122  high-quality BC concentration (Drinovec et al., 2015). The main structure of this algorithm is as follows:

123  $\text{BC (reported)} = \text{BC(zero loading)} \times (1 - k\text{ATN})$  (1)

124  $\text{ATN} = -100 \ln(I/I_0)$  (2)

125      BC1=BC×(1 − $k$ATN1)                                                            (3)

126      BC2=BC×(1 − $k$ATN2)                                                             (4)

127 where BC (reported) is the uncompensated BC concentration; BC (zero loading) is the desired ambient BC value that would

128 be obtained in the absence of any loading effect; $k$ is the loading effect compensation parameter; $I$ and $I_0$ are the light intensity

129 of the measurement spot and reference spot; and ATN is the attenuation of light through filter tape. The BC component of the

130 aerosols is analyzed on two parallel spots drawn from the same input stream in AE-33 but collected at different rates of

131 accumulation. This means that we can obtain different ATN but the same loading parameter $k$ (Drinovec et al., 2015).

132 Combining Eq. (3) and Eq. (4), the compensation parameter $k$ and the desired value of BC compensated back to zero loading

133 can be calculated. Based on the dual-spot technology, the new real-time compensation algorithm allows extrapolation to zero

134 loading and obtains the accurate BC concentration (Drinovec et al., 2015; Crenn et al., 2015; Zhu et al., 2017). Previous studies

135 have evaluated the real-time compensation algorithm of dual-spot Aethalometer model AE-33 and indicated that AE-33 agrees

136 well with the post-processed loading effect compensated data obtained using earlier Aethalometer models and other filter-

137 based absorption photometers, implying the good performance of this new algorithm (Drinovec et al., 2015; Rajesh and

138 Ramachandran, 2018).

139 **2.3 Model simulation and datasets**

140      WRF-Chem version 3.6 was used to analyze the spatial distribution, transport mechanism, and source apportionment of

141 BC during the four observed pollution episodes. The WRF-Chem model is an expansion of the WRF meteorological model

142 and considers complex physical and chemical processes such as emission and deposition, advection and diffusion, gaseous and

143 aqueous chemical transformation, and aerosol chemistry and dynamics (Grell et al., 2005). Here, the numerical experiments

144 were performed at a 25 km horizontal resolution with 122 and 101 grid cells in the west-east and north-south directions,

145 respectively. The simulated domain was centered at 25°N, 82.5°E and had a 30-layer structure with the top pressure of 50 hPa.

146 The key physical and chemical parameterization options for the WRF-Chem model were based on a previous study on the TP

147 (Yang et al., 2018). The initial meteorological fields were taken from the National Centers for Environmental Prediction (NECP)

148 reanalysis data with a horizontal resolution of 1° × 1° at 6 h time intervals. The anthropogenic emission inventory was obtained

149 from the Intercontinental Chemical Transport Experiment-Phase B (INTEX-B) (Zhang et al., 2009) with a resolution of 0.5°

150 × 0.5°. The biogenic emissions were obtained from the Model of Emission of Gases and Aerosol from Nature (MEGAN)

151 (Guenther et al., 2006), and the fire emissions inventory was based on the fire inventory from NCAR (FINN) (Wiedinmyer et

152 al., 2011). Additionally, the Model for Ozone and Related chemical Tracers (MOZART, http://www.acom.ucar.edu/wrf-

153 chem/mozart.shtml) (Emmons et al., 2010) dataset was used to create improved initial and boundary conditions for the BC

154 simulations during these pollution episodes.

155      Furthermore, to predict the source region of BC, we used the Hybrid Single-Particle Lagrangian Integrated Trajectory

156 (HYSPLIT-4) model to calculate the backward trajectories of the air masses (Stein et al., 2015), and the calculation data was

157 obtained from the National Centers for Environmental Prediction/National Center for Atmospheric Research (NCEP/NCAR)

158 reanalysis data ($2.5° \times 2.5°$). The parameter settings for the backward trajectory calculation in the HYSPLIT model were

159 chosen according to a previous study in this area (Xu et al., 2014). The active fire product provided by the Fire Information

160 for Resource Management System (FIRMS, https://firms.modaps.eosdis.nasa.gov/firemap/) was chosen to investigate the

161 biomass burning emissions over the region in different seasons.

## 3. Results and discussion

### 3.1 Temporal variations in BC

#### 3.1.1 Monthly variation in BC

165     The monthly mean BC concentrations at QOMS are shown in Fig. 2a. There was a significant increase in the BC

166 concentrations in winter, and the highest value occurred during the pre-monsoon season ($923.1 \pm 685.8$ ng/m$^3$ in April).

167 Meanwhile, during the monsoon, lower BC concentrations were recorded, and the lowest value was observed in July ($88.5 \pm$

168 $29.8$ ng/m$^3$). This seasonal change was consistent with the previous studies of elemental carbon (EC or BC) at Nepal Climate

169 Observatory-Pyramid station (NCO-P, 27.95°N, 86.82°E, 5079 m a.s.l.) from March 2006 to February 2008 (Fig. 2b) (Marinoni

170 et al., 2010) and at QOMS from August 2009 to July 2010 (Fig. 2c) (Cong et al., 2015a), indicating a similar BC source

171 between the southern and northern sides of the Himalayas. As EC was sampled by quartz filters and detected using the

172 thermal/optical analytical method in previous studies, there may be some differences in the values of EC compared to those of

173 BC, for instance, the overestimation of EC due to the potential effect of carbonates in mineral dust of the samples when using

174 the thermal/optical method (Li et al., 2017a). The monthly variation in EC at Nam Co Monitoring and Research Station for

175 Multisphere Interactions (Nam Co station, 30.77°N, 90.98°E, 4730 m a.s.l.) from January to December during 2012 (Fig. 2d)

176 (Wan et al., 2015) also showed a similar variation, but the peak value of EC occurred in winter. Additionally, the monthly mean

177 EC concentrations at Nam Co station were generally lower than those at QOMS, suggesting that the impact of the

178 anthropogenic activities on the inland TP was weaker than that on the south edge of the TP. Previous studies have demonstrated

179 that the influence of polluted air masses from the "Atmospheric Brown Clouds" over South Asia could reach the southern

180 foothills of the Himalayas and that the mountain-valley breeze circulation carried the polluted air masses onto the TP (Luthi

181 et al., 2015; Cong et al., 2015a; Bonasoni et al., 2008; Yang et al., 2018). Therefore, the seasonal cycle of BC concentrations

182 at QOMS was likely affected by the atmospheric circulation and the emissions from South Asia, which will be further explained

183 in Section 3.3.

#### 3.1.2 Daily variation in BC

Fig. 3 shows the daily mean BC concentrations at QOMS, which present a significant seasonal pattern, with a maximum during the pre-monsoon season (2772.3 ng/m$^3$) and a minimum during the monsoon season (36.4 ng/m$^3$). During the monsoon season, the BC concentration was observed to be lower than 150 ng/m$^3$, but it gradually increased during the post-monsoon and winter. The mean concentration of daily BC at QOMS was 298.8 ± 341.3 ng/m$^3$, which was close to the previous result (250 ± 220 ng/m$^3$) (Cong et al., 2015a).

The comparison between daily mean BC concentrations (Fig. 3) and the meteorological parameters (Fig. S1) suggested that the increasing precipitation during the monsoon led to the washout of atmospheric particles, promoting the wet deposition of BC. This process caused a decrease in BC concentrations during the monsoon, representing the background level during the period. The prevailing wind direction was southwesterly during the monsoon period and westerly during the non-monsoon periods. Therefore, the variations in BC might be linked to the influence of meteorological conditions and the contribution of long-distance transport from urbanized areas to QOMS. Moreover, it cannot be ignored that there were continuous high concentrations of BC above 1000 ng/m$^3$ during 8-10 June 2015, 19-22 March 2016, 9-30 April 2016, and 11-14 April 2017, indicating that the heavy pollution episodes happened at QOMS during those days. A detailed analysis of these pollution events is presented in Section 3.4.

### 3.1.3 Diurnal variation in BC

Diurnal variation characteristics can be used to analyze the impact of local meteorological processes and anthropogenic activities on the BC concentrations at QOMS. The half-hourly mean BC concentrations are presented in Fig. 4. In the pre-monsoon season, the diurnal BC concentrations remained significantly high from late night to morning (00:00-12:00 BJT (Beijing Time: UTC+8h), which is two hours earlier than local time) and increased gradually after the lowest value at approximately 15:30 BJT. Elevated BC concentrations were also observed in the afternoon during the post-monsoon and winter periods, and high BC concentrations occurred from late night to morning. The BC concentrations during the monsoon season were significantly lower than those during the other seasons but peaked in the morning (08:00 BJT) and in the noon (14:00 BJT). Previous studies have demonstrated that the local wind system on the northern slope of Mt. Everest is composed of a morning "valley wind", a late morning-afternoon "glacier wind" weakened by "valley wind", and an evening-early night "mountain wind"(Zou et al., 2008). The QOMS is located in the s-shape valley north of Mt. Everest (Ma et al., 2011). The glacier wind and down mountain wind from the south developed in the afternoon and at night, which provided the potential possibility for pollutants from long-distance sources transported to QOMS along the valley and increased the BC concentrations in the non-monsoon periods. The valley wind from the north in the morning could bring the short-distance emissions from cooking or heating in several villages that are located north (approximately 5 km away) of QOMS. The BC concentrations were remarkably low in the monsoon season but peaked in the morning and in the noon, which might be due to the local emissions carried by the valley wind from the north.

216    To explain the significant high values from late night to morning (00:00-12:00 BJT) in the pre-monsoon season, the wind

217    direction frequency at QOMS during 00:00-12:00 BJT and 12:00-24:00 BJT are presented in Fig. 5. During the sampling

218    period in the pre-monsoon season, W (west) winds prevailed from late night to morning (Fig. 5a), accounting for 18.1% of the

219    total wind directions, followed by ENE (east-northeast) winds (16.4%). This is consistent with the discussion above that there

220    are potential impacts on the BC concentrations at QOMS from long-distance human activity emissions, which can be carried

221    by the westerly winds, i.e., down mountain winds (Cong et al., 2015b). Moreover, the WRF-Chem simulation results showed

222    that the profile of equivalent potential temperature (EPT) increased with altitude and the planetary boundary layer height

223    (PBLH) and wind speed were much lower from late night to morning (Fig. S2), indicating a more stable atmosphere that

224    obstructs the diffusion of BC aerosols. ESE (east-southeast) and NE (northeast) winds prevailed from late morning to night

225    (12:00-24:00 BJT) (Fig. 5b), accounting for 17.6% and 15.3% of the total wind directions, respectively, implying a

226    strengthened glacier wind or mountain wind (from the south), which caused the increase in BC contributed by long-distance

227    sources. During the pre-monsoon season, the strong mountain winds and glacier winds could transport large amounts of trans-

228    Himalayan pollution from heavily polluted areas of South Asia to QOMS; therefore, the long-distance sources play a major

229    role in the diurnal variation in the BC concentrations at QOMS during this period.

230    **3.2 Comparison of the BC concentrations with other sites on the TP**

231    A previous study has revealed that low BC concentrations in China can be found on the TP, with values of approximately

232    200-1000 $ng/m^3$ in $PM_{2.1}$ and 300-1500 $ng/m^3$ in $PM_{9.0}$ (Xin et al., 2015). To better understand the BC loading level, we

233    compared our results with previous studies from other locations over the TP. As shown in Fig. 1, the BC concentrations at

234    Muztagh Ata and Qilian Shan presented low values, which can be regarded as the background concentration level for inland

235    Asia (Cao et al., 2009; Zhao et al., 2012). In contrast, the BC concentration at Lhasa city was higher than that at other sites on

236    the TP, which was mainly contributed by local fossil fuel combustion (Li et al., 2016b). In addition, under the impact of the

237    long-range transport of anthropogenic emissions from the east and significant dust input from the west, the BC concentration

238    at Qinghai Lake also showed a relatively high value (Li et al., 2013). The BC concentration at Beiluhe was slightly higher than

239    that at Qinghai Lake, mainly from the arid regions in northwestern China in spring and from the southern slope of the

240    Himalayas in winter (Wang et al., 2016). Therefore, the long-range transportation from Central Asia and East Asia contributed

241    greatly to the BC aerosols in the northern TP. For the sites in the central and southeastern regions on the TP (e.g., Nam Co and

242    Ranwu), which are isolated from anthropogenic activities with relatively clean atmospheric environments, the BC

243    concentrations at these two sites were above 130 $ng/m^3$, likely due to the influence of long-range transport from South Asia

244    (Wan et al., 2015; Wang et al., 2016). Compared with the locations on the southern slope of the Himalayas (e.g., NCO-P and

245    Manora Peak), the BC concentration at QOMS was close to that at NCO-P but much lower than that at Manora Peak, which is

246    near the polluted areas in South Asia and largely affected by anthropogenic emissions (Marinoni et al., 2010; Ram et al., 2010).

247   This implies that the combustion emissions from South Asia affect not only the lower latitudes in the vicinity but also the

248   higher latitudes in the Himalayas and the interior of the TP due to long-range transport.

**3.3 Potential sources and transport mechanisms of BC in different seasons**

250      The seasonal variation in the BC concentrations was correlated with the combustion intensity of sources and atmospheric

251   circulation. The "Atmospheric Brown Clouds" over South Asia contain large amounts of aerosol components such as the high

252   loading emissions of BC from biomass burning, which can reach the TP within a few days (Ramanathan et al., 2005;

253   Ramanathan and Ramana, 2005; Luthi et al., 2015). A previous study has quantified biomass burning sources contributing to

254   BC aerosols from the Himalayan region of Nepal and India and showed that the major fires were concentrated from March to

255   June; additionally, most fires occurred in the low elevation areas dominated by forests and croplands (Vadrevu et al., 2012).

256   Therefore, we further checked the biomass burning emissions in the Mt. Everest region and its vicinities using the active fire

257   product from the MODIS data during four seasons (August 2015 to April 2016) provided by the FIRMS (Fig. 6). It is clearly

258   shown that there were large numbers of active fire spots in northern and central India, Pakistan and Nepal in winter and in the

259   pre-monsoon season. Moreover, referring to Cong et al. (2015a), the active fire spots represent agricultural combustion and

260   forest fires in this region, which might substantially contribute to BC aerosols. During the monsoon season, insignificant fire

261   spots appeared in South Asia, representing less biomass burning in that period.

262      To further explore the sources and the long-range transport mechanism of BC aerosols at QOMS, we calculated the

263   frequency plots for 5-day backward trajectories arriving 1 km above ground level (Fig. 7). During the non-monsoon seasons,

264   the air masses were affected by the westerly winds. The air masses reaching the Mt. Everest region were mostly from the

265   northwest, indicating that the biomass burning emissions in Pakistan, northern India and Nepal could be transported to the Mt.

266   Everest region. However, for the difference in the combustion intensity, high concentrations of BC were found only during the

267   pre-monsoon season. During the monsoon season, the southerly winds dominated in the Mt. Everest region, and the air masses

268   were mainly from the Arabian Sea and the Bay of Bengal with substantial moisture. At this period, the precipitation on the

269   southern side of the Himalayas was above 1200 mm (Xu et al., 2014), which can improve the wet removal efficiency of BC.

270   Moreover, the biomass combustion emissions in South Asia in this period were very low. Therefore, the BC concentrations at

271   QOMS were close to the background level during the monsoon season. Meanwhile, the local meteorological conditions also

272   play a very important role in the transport of pollutants across the Himalayas from South Asia. Previous studies have shown

273   that the local wind system was mainly composed of up-valley wind on the southern slope and down-valley wind on the northern

274   slope, which facilitates the exchange of air between the bottom and upside of the atmosphere, and facilitates the coupling of

275   air flow between the southern and northern slopes, which allows the pollutants from South Asia to easily cross the Himalayas

276   and be transported to the TP from the valley (Zou et al., 2008; Chen et al., 2012; Cong et al., 2015b; Tripathee et al., 2017;

277   Dhungel et al., 2018).

## 3.4 Pollution episodes analysis by WRF-Chem modeling

In this section, we analyzed four pollution events with BC concentrations above 1000 ng/m$^3$ in detail, including event A during 8-10 June 2015, event B during 19-22 March 2016, event C during 9-30 April 2016, and event D during 11-14 April 2017. Fig. 8 shows the spatial characteristics of the WRF-Chem modeled surface BC concentrations during the four pollution episodes. It can be seen that the high values of surface BC concentrations always appeared in South Asia, although the high-value centers changed in different pollution events. For event A, the most serious pollution appeared in Nepal and northern India. There was relatively less BC near Mt. Everest in event B than in the other events. However, for event C, the high BC concentration areas were mainly along the southern slope of the Himalayas in Nepal and eastern India, which can highly impact the BC concentrations in the Mt. Everest region. In event D, the high BC concentrations occurred in Nepal and some parts of India. To evaluate the model performance, the temporal variation in measured and simulated BC concentrations at QOMS during these four pollution episodes are displayed in Fig. S3. As shown in Fig. S3, for the four pollution episodes, the WRF-Chem model captured the variation trends of the observed BC concentrations, with correlation coefficients all above 0.8. This implies that the model could reproduce the distribution of BC concentrations in this region. Additionally, comparisons between the modeled wind and precipitation and the wind and precipitation from reanalysis data and in-situ observations indicated that the WRF-Chem model could capture the spatiotemporal variations in the meteorological elements (Fig. S4 and Fig. S5).

The sources and transport mechanisms of BC aerosols during these pollution episodes can be indicated by analyzing the air flow. Fig. 9 shows the variation in the BC concentrations and wind fields at different altitudes in the atmosphere (850 hPa, 500 hPa, and 200 hPa). For event A during the monsoon season, there was a cyclone in northern India at 850 hPa that moved near-surface BC aerosols upward, and then, the southerly winds at 500 hPa and 200 hPa transported the BC aerosols to the Mt. Everest region. For events B-D in the pre-monsoon season, the northwesterly winds prevailed in South Asia at 850 hPa and brought BC from northern India to the southern slope of the Himalayas, and the westerly winds at 500 hPa and 200 hPa transported relatively less BC from northwestern India and Central Asia to the Mt. Everest region. Previous studies also pointed out that BC can be transported across the Himalayas to the Mt. Everest region by the mountain-valley wind system (Zou et al., 2008; Cong et al., 2015b; Dhungel et al., 2018). Thus, we needed to further analyze the impact of the mountain-valley wind on the transportation of BC. Fig. 10 shows the vertical profile of the BC concentration along the QOMS's longitude of 86.95°E. During event A, high concentrations of BC appeared in the upper atmosphere of South Asia, and many BC aerosols were transported to most parts of the TP (Fig. 10a) due to the large-scale transport process. However, for events B-D, high concentrations of BC occurred along the southern slope of the Himalayas, and BC aerosols were only transported to a few areas on the northern slope of the Himalayas such as the Mt. Everest region (Fig. 10b-d) due to the local mountain-valley wind. As shown in Fig. S6, for events B-D, the up-valley wind on the southern side of the Himalayas can move BC aerosols up in the daytime, and the down-valley wind can cause the aerosols to descend in the Mt. Everest region at night.

309   To sum up, we found that the transport processes of BC aerosols from South Asia to the QOMS were different as the

310   seasons changed. In the monsoon season such as event A, BC aerosols were moved upward by the cyclone in the lower

311   atmosphere and were transported to QOMS by the southerly winds in the upper atmosphere. However, in the pre-monsoon

312   season such as events B-D, the mountain-valley wind played an important role in transporting the BC aerosols from the

313   southern slope of the Himalayas to the Mt. Everest region.

314   **4. Conclusions**

315   In this study, BC concentrations were measured from 15 May 2015 to 31 May 2017 at QOMS on the south edge of the

316   TP. Monthly, daily, and diurnal variations in BC concentrations were calculated to investigate the temporal characteristics and

317   potential sources of BC at QOMS. The results showed that the monthly mean BC concentrations reached the highest value in

318   the pre-monsoon season (923.1 $\pm$685.8 ng/m$^3$) and the lowest value in the monsoon season (88.5 $\pm$29.8 ng/m$^3$). The average

319   daily BC concentration was equal to 298.8 $\pm$ 341.3 ng/m$^3$, with a maximum in the pre-monsoon season (2772.3 ng/m$^3$) and a

320   minimum in the monsoon season (36.4 ng/m$^3$). For the diurnal variation in BC, there was an increase in the afternoon during

321   the non-monsoon periods, and high BC concentrations occurred from late night to morning, implying that the potential origin

322   of BC was from long-range transport. The BC concentrations remained low but peaked in the morning and in the noon during

323   the monsoon period, which might be due to local anthropogenic activities. In addition, the substantially high values of diurnal

324   variation in the BC concentrations in the pre-monsoon season suggest the high contributions of long-distance emissions carried

325   by mountain winds and glacier winds.

326   The seasonal cycle of BC concentrations at QOMS was closely correlated with the variation in the atmospheric circulation

327   and combustion emissions in South Asia. In the non-monsoon seasons, affected by the westerly winds, the air masses in the

328   Mt. Everest region were largely from Pakistan, northern Indian, and Nepal due to the high loading emissions from vegetation

329   fires. In the monsoon season, the southerly winds prevailed in the Mt. Everest region, and the air masses were mainly from the

330   Arabian Sea and the Bay of Bengal. Under intense precipitation scavenging of BC and extremely low levels of combustion

331   emissions in South Asia, the BC concentrations at QOMS were close to the background level in the monsoon season.

332   For the four heavy pollution episodes that occurred at QOMS with BC concentrations above 1000 ng/m$^3$, we found that

333   the transport processes of the BC aerosols from South Asia to the Mt. Everest region were different as the seasons changed. In

334   the monsoon season (using the pollution event during 8-10 June 2015 as an example), BC aerosols were efficiently driven

335   upward by the cyclone in the lower atmosphere in South Asia and transported to the Mt. Everest region by the southerly winds

336   in the upper atmosphere. However, during the pre-monsoon season (using the other three pollution events as examples), the

337   mountain-valley wind played an important role in transporting the BC aerosols across the Himalayas to the Mt. Everest region.

338   *Data availability.* All data are available upon requests made to the corresponding author.

339    *Competing interests.* The authors declare that they have no conflict of interest.

340    *Special issue statement.* This article is part of the special issue "Study of ozone, aerosols and radiation over the Tibetan Plateau

341    (SOAR-TP) (ACP/AMT inter-journal SI)". It is not associated with a conference.

342    *Acknowledgments.* This study was supported by the National Nature Science Foundation of China (41630754, 41675130,

343    41721091), Chinese Academy of Sciences (QYZDJ-SSW-DQC039), and State Key Laboratory of Cryospheric Science

344    (SKLCS-ZZ-2017). The authors thank the staff of the Qomolangma Atmospheric and Environmental Observation and

345    Research Station of Chinese Academy of Sciences for collecting data and the support of meteorological dataset. We also give

346    thanks to Tony Hansen for his suggestion on data processing and Xin Wan, Lekhendra Tripathee, and Yajun Liu for their help

347    to improve the quality of this paper.

348 **References**

349 Anenberg, S. C., Schwartz, J., Shindell, D., Amann, M., Faluvegi, G., Klimont, Z., Janssens-Maenhout, G., Pozzoli, L., Van

350 Dingenen, R., Vignati, E., Emberson, L., Muller, N. Z., West, J. J., Williams, M., Demkine, V., Hicks, W. K., Kuylenstierna,

351 J., Raes, F., and Ramanathan, V.: Global air quality and health co-benefits of mitigating near-term climate change through

352 methane and black carbon emission controls, Environ. Health Perspect., 120, 831-839,

353 https://doi.org/10.1289/ehp.1104301, 2012.

354 Bonasoni, P., Laj, P., Angelini, F., Arduini, J., Bonafe, U., Calzolari, F., Cristofanelli, P., Decesari, S., Facchini, M. C., Fuzzi,

355 S., Gobbi, G. P., Maione, M., Marinoni, A., Petzold, A., Roccato, F., Roger, J. C., Sellegri, K., Sprenger, M., Venzac, H.,

356 Verza, G. P., Villani, P., and Vuillermoz, E.: The ABC-Pyramid Atmospheric Research Observatory in Himalaya for aerosol,

357 ozone and halocarbon measurements, Sci. Total Environ., 391, 252-261, https://doi.org/10.1016/j.scitotenv.2007.10.024,

358 2008.

359 Bond, T. C., Anderson, T. L., and Campbell, D.: Calibration and intercomparison of filter-based measurements of visible light

360 absorption by aerosols, Aerosol Sci. Technol., 30, 582-600, https://doi.org/10.1080/027868299304435, 1999.

361 Bond, T. C.: A technology-based global inventory of black and organic carbon emissions from combustion, J. Geophys. Res.,

362 109, https://doi.org/10.1029/2003jd003697, 2004.

363 Bond, T. C., Doherty, S. J., Fahey, D. W., Forster, P. M., Berntsen, T., DeAngelo, B. J., Flanner, M. G., Ghan, S., Kärcher, B.,

364 Koch, D., Kinne, S., Kondo, Y., Quinn, P. K., Sarofim, M. C., Schultz, M. G., Schulz, M., Venkataraman, C., Zhang, H.,

365 Zhang, S., Bellouin, N., Guttikunda, S. K., Hopke, P. K., Jacobson, M. Z., Kaiser, J. W., Klimont, Z., Lohmann, U., Schwarz,

366 J. P., Shindell, D., Storelvmo, T., Warren, S. G., and Zender, C. S.: Bounding the role of black carbon in the climate system:

367 A scientific assessment, J. Geophys. Res.: Atmos., 118, 5380-5552, https://doi.org/10.1002/jgrd.50171, 2013.

368 Cao, J., Xu, B., He, J., Liu, X., Han, Y., Wang, G., and Zhu, C.: Concentrations, seasonal variations, and transport of

369 carbonaceous aerosols at a remote Mountainous region in western China, Atmos. Environ., 43, 4444-4452,

370 https://doi.org/10.1016/j.atmosenv.2009.06.023, 2009.

371 Chen, X., Su, Z., Ma, Y., and Sun, F.: Analysis of Land-Atmosphere Interactions over the North Region of Mt. Qomolangma

372 (Mt. Everest), Arct. Antarct. Alp. Res., 44, 412-4222012.

373 Chow, J. C., Watson, J. G., Pritchett, L. C., Pierson, W. R., Frazier, C. A., and Purcell, R. G.: The DRI thermal/optical

374 reflectance carbon analysis system: description, evaluation and applications in U.S. air quality studies, Atmos. Environ.,

375 27, 1185-1201, https://doi.org/https://doi.org/10.1016/0960-1686(93)90245-T, 1993.

376 Chow, J. C., Watson, J. G., Crow, D., Lowenthal, D. H., and Merrifield, T.: Comparison of IMPROVE and NIOSH carbon

377 measurements, Aerosol Sci. Technol., 34, 23-34, https://doi.org/10.1080/027868201300081923, 2001.

378 Cong, Z., Kang, S., Kawamura, K., Liu, B., Wan, X., Wang, Z., Gao, S., and Fu, P.: Carbonaceous aerosols on the south edge

379    of the Tibetan Plateau: concentrations, seasonality and sources, Atmos. Chem. Phys., 15, 1573-1584,

380    https://doi.org/10.5194/acp-15-1573-2015, 2015a.

381    Cong, Z., Kawamura, K., Kang, S., and Fu, P.: Penetration of biomass-burning emissions from South Asia through the

382    Himalayas: new insights from atmospheric organic acids, Sci. Rep., 5, 9580, https://doi.org/10.1038/srep09580, 2015b.

383    Cooke, W. F., Ramaswamy, V., and Kasibhatla, P.: A general circulation model study of the global carbonaceous aerosol

384    distribution, J. Geophys. Res.: Atmos., 107, ACH 2-1-ACH 2-32, https://doi.org/10.1029/2001JD001274, 2002.

385    Crenn, V., Sciare, J., Croteau, P. L., Verlhac, S., Froehlich, R., Belis, C. A., Aas, W., Aijala, M., Alastuey, A., Artinano, B.,

386    Baisnee, D., Bonnaire, N., Bressi, M., Canagaratna, M., Canonaco, F., Carbone, C., Cavalli, F., Coz, E., Cubison, M. J.,

387    Esser-Gietl, J. K., Green, D. C., Gros, V., Heikkinen, L., Herrmann, H., Lunder, C., Minguillon, M. C., Mocnik, G., O'Dowd,

388    C. D., Ovadnevaite, J., Petit, J. E., Petralia, E., Poulain, L., Priestman, M., Riffault, V., Ripoll, A., Sarda-Esteve, R., Slowik,

389    J. G., Setyan, A., Wiedensohler, A., Baltensperger, U., Prevot, A. S. H., Jayne, J. T., and Favez, O.: ACTRIS ACSM

390    intercomparison - Part 1: Reproducibility of concentration and fragment results from 13 individual Quadrupole Aerosol

391    Chemical Speciation Monitors (Q-ACSM) and consistency with co-located instruments, Atmos. Meas. Tech., 8, 5063-5087,

392    https://doi.org/10.5194/amt-8-5063-2015, 2015.

393    Dhungel, S., Kathayat, B., Mahata, K., and Panday, A.: Transport of regional pollutants through a remote trans-Himalayan

394    valley in Nepal, Atmos. Chem. Phys., 18, 1203-1216, https://doi.org/10.5194/acp-18-1203-2018, 2018.

395    Drinovec, L., Mocnik, G., Zotter, P., Prevot, A. S. H., Ruckstuhl, C., Coz, E., Rupakheti, M., Sciare, J., Mueller, T.,

396    Wiedensohler, A., and Hansen, A. D. A.: The "dual-spot" Aethalometer: an improved measurement of aerosol black carbon

397    with real-time loading compensation, Atmos. Meas. Tech., 8, 1965-1979, https://doi.org/10.5194/amt-8-1965-2015, 2015.

398    Emmons, L. K., Walters, S., Hess, P. G., Lamarque, J. F., Pfister, G. G., Fillmore, D., Granier, C., Guenther, A., Kinnison, D.,

399    Laepple, T., Orlando, J., Tie, X., Tyndall, G., Wiedinmyer, C., Baughcum, S. L., and Kloster, S.: Description and evaluation

400    of the Model for Ozone and Related chemical Tracers, version 4 (MOZART-4), Geosci. Model Dev., 3, 43-67,

401    https://doi.org/10.5194/gmd-3-43-2010, 2010.

402    Fialho, P., Hansen, A. D. A., and Honrath, R. E.: Absorption coefficients by aerosols in remote areas: a new approach to

403    decouple dust and black carbon absorption coefficients using seven-wavelength Aethalometer data, J. Aerosol Sci., 36,

404    267-282, https://doi.org/10.1016/j.jaerosci.2004.09.004, 2005.

405    Flanner, M. G., Zender, C. S., Randerson, J. T., and Rasch, P. J.: Present-day climate forcing and response from black carbon

406    in snow, J. Geophys. Res., 112, https://doi.org/10.1029/2006jd008003, 2007.

407    Gao, X., Shi, Y., Song, R., Giorgi, F., Wang, Y., and Zhang, D.: Reduction of future monsoon precipitation over China:

408    comparison between a high resolution RCM simulation and the driving GCM, Meteorol. Atmos. Phys., 100, 73-86,

409    https://doi.org/10.1007/s00703-008-0296-5, 2008.

410    Grell, G. A., Peckham, S. E., Schmitz, R., McKeen, S. A., Frost, G., Skamarock, W. C., and Eder, B.: Fully coupled "online"

411    chemistry within the WRF model, Atmos. Environ., 39, 6957-6975, https://doi.org/10.1016/j.atmosenv.2005.04.027, 2005.

412    Guenther, A., Karl, T., Harley, P., Wiedinmyer, C., Palmer, P. I., and Geron, C.: Estimates of global terrestrial isoprene

413    emissions using MEGAN (Model of Emissions of Gases and Aerosols from Nature), Atmos. Chem. Phys., 6, 3181-3210,

414    https://doi.org/10.5194/acp-6-3181-2006, 2006.

415    Hansen, A. D. A., Rosen, H., and Novakov, T.: The aethalometer — An instrument for the real-time measurement of optical

416    absorption by aerosol particles, Sci. Total Environ., 36, 191-196, https://doi.org/10.1016/0048-9697(84)90265-1, 1984.

417    Hansen, J., Sato, M., Ruedy, R., Lacis, A., and Oinas, V.: Global warming in the twenty-first century: An alternative scenario,

418    Proc. Natl. Acad. Sci. U. S. A., 97, 9875-9880, https://doi.org/10.1073/pnas.170278997, 2000.

419    He, C., Li, Q., Liou, K. N., Takano, Y., Gu, Y., Qi, L., Mao, Y., and Leung, L. R.: Black carbon radiative forcing over the

420    Tibetan Plateau, Geophys. Res. Lett., 41, 7806-7813, https://doi.org/doi:10.1002/2014GL062191, 2014a.

421    He, C., Li, Q., Liou, K. N., Zhang, J., Qi, L., Mao, Y., Gao, M., Lu, Z., Streets, D. G., Zhang, Q., Sarin, M. M., and Ram, K.:

422    A global 3-D CTM evaluation of black carbon in the Tibetan Plateau, Atmos. Chem. Phys., 14, 7091-7112,

423    https://doi.org/10.5194/acp-14-7091-2014, 2014b.

424    He, C., Takano, Y., Liou, K.-N., Yang, P., Li, Q., and Chen, F.: Impact of Snow Grain Shape and Black Carbon–Snow Internal

425    Mixing on Snow Optical Properties: Parameterizations for Climate Models, J. Clim., 30, 10019-10036,

426    https://doi.org/10.1175/jcli-d-17-0300.1, 2017.

427    Hyvarinen, A. P., Vakkari, V., Laakso, L., Hooda, R. K., Sharma, V. P., Panwar, T. S., Beukes, J. P., van Zyl, P. G., Josipovic,

428    M., Garland, R. M., Andreae, M. O., Poeschl, U., and Petzold, A.: Correction for a measurement artifact of the Multi-Angle

429    Absorption Photometer (MAAP) at high black carbon mass concentration levels, Atmos. Meas. Tech., 6, 81-90,

430    https://doi.org/10.5194/amt-6-81-2013, 2013.

431    Jacobson, M. Z.: Strong radiative heating due to the mixing state of black carbon in atmospheric aerosols, Nature, 409, 695-

432    697, https://doi.org/10.1038/35055518, 2001.

433    Jacobson, M. Z.: Control of fossil-fuel particulate black carbon and organic matter, possibly the most effective method of

434    slowing global warming, J. Geophys. Res., 107, https://doi.org/10.1029/2001JD001376, 2002.

435    Ji, Z., Kang, S., Cong, Z., Zhang, Q., and Yao, T.: Simulation of carbonaceous aerosols over the Third Pole and adjacent regions:

436    distribution, transportation, deposition, and climatic effects, Clim. Dyn., 45, 2831-2846, https://doi.org/10.1007/s00382-

437    015-2509-1, 2015.

438    Ji, Z.: Modeling black carbon and its potential radiative effects over the Tibetan Plateau, Adv. Clim. Change. Res., 7, 139-144,

439    https://doi.org/10.1016/j.accre.2016.10.002, 2016.

440    Jurado, E., Dachs, J., Duarte, C. M., and Simó, R.: Atmospheric deposition of organic and black carbon to the global oceans,

441    Atmos. Environ., 42, 7931-7939, https://doi.org/10.1016/j.atmosenv.2008.07.029, 2008.

442    Kang, S., Xu, Y., You, Q., Fluegel, W.-A., Pepin, N., and Yao, T.: Review of climate and cryospheric change in the Tibetan

443    Plateau, Environ. Res. Lett., 5, 015101, https://doi.org/10.1088/1748-9326/5/1/015101, 2010.

444    Kang, S., Chen, P., Li, C., Liu, B., and Cong, Z.: Atmospheric Aerosol Elements over the Inland Tibetan Plateau: Concentration,

445       Seasonality, and Transport, Aerosol Air Qual. Res., 16, 789-800, https://doi.org/10.4209/aaqr.2015.05.0307, 2016.

446    Kopacz, M., Mauzerall, D. L., Wang, J., Leibensperger, E. M., Henze, D. K., and Singh, K.: Origin and radiative forcing of

447       black carbon transported to the Himalayas and Tibetan Plateau, Atmos. Chem. Phys., 11, 2837-2852,

448       https://doi.org/10.5194/acp-11-2837-2011, 2011.

449    Laborde, M., Schnaiter, M., Linke, C., Saathoff, H., Naumann, K. H., Mohler, O., Berlenz, S., Wagner, U., Taylor, J. W., Liu,

450       D., Flynn, M., Allan, J. D., Coe, H., Heimerl, K., Dahlkotter, F., Weinzierl, B., Wollny, A. G., Zanatta, M., Cozic, J., Laj,

451       P., Hitzenberger, R., Schwarz, J. P., and Gysel, M.: Single Particle Soot Photometer intercomparison at the AIDA chamber,

452       Atmos. Meas. Tech., 5, 3077-3097, https://doi.org/10.5194/amt-5-3077-2012, 2012.

453    Lee, W. L., Liou, K. N., He, C. L., Liang, H. C., Wang, T. C., Li, Q. B., Liu, Z. X., and Yue, Q.: Impact of absorbing aerosol

454       deposition on snow albedo reduction over the southern Tibetan plateau based on satellite observations, Theor. Appl.

455       Climatol., 129, 1373-1382, https://doi.org/10.1007/s00704-016-1860-4, 2017.

456    Li, C., Bosch, C., Kang, S., Andersson, A., Chen, P., Zhang, Q., Cong, Z., Chen, B., Qin, D., and Gustafsson, O.: Sources of

457       black carbon to the Himalayan-Tibetan Plateau glaciers, Nat. Commun., 7, 12574, https://doi.org/10.1038/ncomms12574,

458       2016a.

459    Li, C., Chen, P., Kang, S., Yan, F., Hu, Z., Qu, B., and Sillanpää, M.: Concentrations and light absorption characteristics of

460       carbonaceous aerosol in PM 2.5 and PM 10 of Lhasa city, the Tibetan Plateau, Atmos. Environ., 127, 340-346,

461       https://doi.org/10.1016/j.atmosenv.2015.12.059, 2016b.

462    Li, C., Yan, F., Kang, S., Chen, P., Han, X., Hu, Z., Zhang, G., Hong, Y., Gao, S., Qu, B., Zhu, Z., Li, J., Chen, B., and Sillanpää,

463       M.: Re-evaluating black carbon in the Himalayas and the Tibetan Plateau: concentrations and deposition, Atmos. Chem.

464       Phys., 17, 11899-11912, https://doi.org/10.5194/acp-17-11899-2017, 2017a.

465    Li, J., Wang, G., Wang, X., Cao, J., Sun, T., Cheng, C., Meng, J., Hu, T., and Liu, S.: Abundance, composition and source of

466       atmospheric PM2.5 at a remote site in the Tibetan Plateau, China, Tellus B, 65, 20281,

467       https://doi.org/10.3402/tellusb.v65i0.20281, 2013.

468    Li, X., Kang, S., He, X., Qu, B., Tripathee, L., Jing, Z., Paudyal, R., Li, Y., Zhang, Y., Yan, F., Li, G., and Li, C.: Light-

469       absorbing impurities accelerate glacier melt in the Central Tibetan Plateau, Sci. Total Environ., 587, 482-490,

470       https://doi.org/10.1016/j.scitotenv.2017.02.169, 2017b.

471    Li, X., Kang, S., Zhang, G., Qu, B., Tripathee, L., Paudyal, R., Jing, Z., Zhang, Y., Yan, F., Li, G., Cui, X., Xu, R., Hu, Z., and

472       Li, C.: Light-absorbing impurities in a southern Tibetan Plateau glacier: Variations and potential impact on snow albedo

473       and radiative forcing, Atmos. Res., 200, 77-87, https://doi.org/10.1016/j.atmosres.2017.10.002, 2018.

474    Lu, A., Kang, S., Li, Z., and Theakstone, W. H.: Altitude effects of climatic variation on Tibetan Plateau and its vicinities, J.

Earth Sci., 21, 189-198, https://doi.org/10.1007/s12583-010-0017-0, 2010.

Lu, Z., Streets, D. G., Zhang, Q., and Wang, S.: A novel back-trajectory analysis of the origin of black carbon transported to the Himalayas and Tibetan Plateau during 1996-2010, Geophys. Res. Lett., 39, L01809, https://doi.org/10.1029/2011gl049903, 2012.

Luthi, Z. L., Skerlak, B., Kim, S. W., Lauer, A., Mues, A., Rupakheti, M., and Kang, S.: Atmospheric brown clouds reach the Tibetan Plateau by crossing the Himalayas, Atmos. Chem. Phys., 15, 6007-6021, https://doi.org/10.5194/acp-15-6007-2015, 2015.

Ma, Y., Wang, Y., Zhong, L., Wu, R., Wang, S., and Li, M.: The Characteristics of Atmospheric Turbulence and Radiation Energy Transfer and the Structure of Atmospheric Boundary Layer over the Northern Slope Area of Himalaya, J. Meteorol. Soc. Jpn., 89A, 345-353, https://doi.org/10.2151/jmsj.2011-A24, 2011.

Marinoni, A., Cristofanelli, P., Laj, P., Duchi, R., Calzolari, F., Decesari, S., Sellegri, K., Vuillermoz, E., Verza, G. P., Villani, P., and Bonasoni, P.: Aerosol mass and black carbon concentrations, a two year record at NCO-P (5079 m, Southern Himalayas), Atmos. Chem. Phys., 10, 8551-8562, https://doi.org/10.5194/acp-10-8551-2010, 2010.

Menon, S., Koch, D., Beig, G., Sahu, S., Fasullo, J., and Orlikowski, D.: Black carbon aerosols and the third polar ice cap, Atmos. Chem. Phys., 10, 4559-4571, https://doi.org/10.5194/acp-10-4559-2010, 2010.

Ming, J., Cachier, H., Xiao, C., Qin, D., Kang, S., Hou, S., and Xu, J.: Black carbon record based on a shallow Himalayan ice core and its climatic implications, Atmos. Chem. Phys., 8, 1343-1352, https://doi.org/10.5194/acp-8-1343-2008, 2008.

Oshima, N., Kondo, Y., Moteki, N., Takegawa, N., Koike, M., Kita, K., Matsui, H., Kajino, M., Nakamura, H., Jung, J. S., and Kim, Y. J.: Wet removal of black carbon in Asian outflow: Aerosol Radiative Forcing in East Asia (A-FORCE) aircraft campaign, J. Geophys. Res., 117, D03204, https://doi.org/10.1029/2011jd016552, 2012.

Park, S. S., Hansen, A. D. A., and Cho, S. Y.: Measurement of real time black carbon for investigating spot loading effects of Aethalometer data, Atmos. Environ., 44, 1449-1455, https://doi.org/10.1016/j.atmosenv.2010.01.025, 2010.

Petzold, A., and Schonlinner, M.: Multi-angle absorption photometry - a new method for the measurement of aerosol light absorption and atmospheric black carbon, J. Aerosol Sci., 35, 421-441, https://doi.org/10.1016/j.jaerosci.2003.09.005, 2004.

Praveen, P. S., Ahmed, T., Kar, A., Rehman, I. H., and Ramanathan, V.: Link between local scale BC emissions and large scale atmospheric solar absorption, Atmos. Chem. Phys., 12, 1173-1187, https://doi.org/10.5194/acp-12-1173-2012, 2012.

Qu, B., Ming, J., Kang, S.-C., Zhang, G.-S., Li, Y.-W., Li, C.-D., Zhao, S.-Y., Ji, Z.-M., and Cao, J.-J.: The decreasing albedo of Zhadang glacier on western Nyainqentanglha and the role of light-absorbing impurities, Atmos. Chem. Phys., 14, 11117-11128, https://doi.org/10.5194/acp-14-11117-2014, 2014.

Rajesh, T. A., and Ramachandran, S.: Black carbon aerosol mass concentration, absorption and single scattering albedo from single and dual spot aethalometers: Radiative implications, J. Aerosol Sci., 119, 77-90,

507 https://doi.org/10.1016/j.jaerosci.2018.02.001, 2018.

508 Ram, K., Sarin, M. M., and Hegde, P.: Long-term record of aerosol optical properties and chemical composition from a high-

509 altitude site (Manora Peak) in Central Himalaya, Atmos. Chem. Phys., 10, 11791-11803, https://doi.org/10.5194/acp-10-

510 11791-2010, 2010.

511 Ramanathan, V., Chung, C., Kim, D., Bettge, T., Buja, L., Kiehl, J. T., Washington, W. M., Fu, Q., Sikka, D. R., and Wild, M.:

512 Atmospheric brown clouds: impacts on South Asian climate and hydrological cycle, P. Natl. Acad. Sci. USA, 102, 5326-

513 5333, https://doi.org/10.1073/pnas.0500656102, 2005.

514 Ramanathan, V., and Ramana, M. V.: Persistent, Widespread, and Strongly Absorbing Haze Over the Himalayan Foothills and

515 the Indo-Gangetic Plains, Pure appl. geophys., 162, 1609-1626, https://doi.org/10.1007/s00024-005-2685-8, 2005.

516 Ramanathan, V., and Carmichael, G.: Global and Regional Climate Changes Due to Black Carbon, Nature Geosci., 1, 221-227,

517 https://doi.org/10.1038/ngeo156, 2008.

518 Sandradewi, J., Prevot, A., Szidat, S., Perron, N., Alfarra, M., A Lanz, V., Weingartner, E., and Baltensperger, U.: Using aerosol

519 light absorption measurements for the quantitative determination of wood burning and traffic emission contributions to

520 particulate matter, Environ. Sci. Technol., 42, 3316-3323, https://doi.org/10.1021/es702253m, 2008a.

521 Sandradewi, J., Prevot, A., Weingartner, E., Schmidhauser, R., Gysel, M., and Baltensperger, U.: A study of wood burning and

522 traffic aerosols in an Alpine valley using a multi-wavelength Aethalometer, Atmos. Environ., 42, 101-112,

523 https://doi.org/10.1016/j.atmosenv.2007.09.034, 2008b.

524 Schauer, J. J., Mader, B. T., Deminter, J. T., Heidemann, G., Bae, M. S., Seinfeld, J. H., Flagan, R. C., Cary, R. A., Smith, D.,

525 Huebert, B. J., Bertram, T., Howell, S., Kline, J. T., Quinn, P., Bates, T., Turpin, B., Lim, H. J., Yu, J. Z., Yang, H., and

526 Keywood, M. D.: ACE-Asia intercomparison of a thermal-optical method for the determination of particle-phase organic

527 and elemental carbon, Environ. Sci. Technol., 37, 993-1001, https://doi.org/10.1021/es020622f, 2003.

528 Schwarz, J. P., Spackman, J. R., Gao, R. S., Perring, A. E., Cross, E., Onasch, T. B., Ahern, A., Wrobel, W., Davidovits, P.,

529 Olfert, J., Dubey, M. K., Mazzoleni, C., and Fahey, D. W.: The Detection Efficiency of the Single Particle Soot Photometer,

530 Aerosol Sci. Technol., 44, 612-628, https://doi.org/10.1080/02786826.2010.481298, 2010.

531 Skamarock, W. C., Klemp, J. B., Dudhia, J., Gill, D. O., Barker, D. M., Wang, W., and Powers, J. G.: A Description of the

532 Advanced Research WRF Version 2, NCAR Technical Note NCAR/TN-468+STR, https://doi.org/doi:10.5065/D6DZ069T,

533 2005.

534 Stein, A. F., Draxler, R. R., Rolph, G. D., Stunder, B. J. B., Cohen, M. D., and Ngan, F.: NOAA'S HYSPLIT ATMOSPHERIC

535 TRANSPORT AND DISPERSION MODELING SYSTEM, Bull. Am. Meteorol. Soc., 96, 2059-2077,

536 https://doi.org/10.1175/bams-d-14-00110.1, 2015.

537 Stephens, M., Turner, N., and Sandberg, J.: Particle identification by laser-induced incandescence in a solid-state laser cavity,

538 Appl. Opt., 42, 3726-3736, https://doi.org/10.1364/ao.42.003726, 2003.

539  Tripathee, L., Kang, S., Rupakheti, D., Cong, Z., Zhang, Q., and Huang, J.: Chemical characteristics of soluble aerosols over

540      the central Himalayas: insights into spatiotemporal variations and sources, Environ. Sci. Pollut. Res., 24, 24454-24472,

541      https://doi.org/10.1007/s11356-017-0077-0, 2017.

542  Vadrevu, K. P., Ellicott, E., Giglio, L., Badarinath, K. V. S., Vermote, E., Justice, C., and Lau, W. K. M.: Vegetation fires in the

543      himalayan region – Aerosol load, black carbon emissions and smoke plume heights, Atmos. Environ., 47, 241-251,

544      https://doi.org/10.1016/j.atmosenv.2011.11.009, 2012.

545  Virkkula, A., Makela, T., Hillamo, R., Yli-Tuomi, T., Hirsikko, A., Hameri, K., and Koponen, I. K.: A simple procedure for

546      correcting loading effects of aethalometer data, J. Air Waste Manage. Assoc., 57, 1214-1222, https://doi.org/10.3155/1047-

547      3289.57.10.1214, 2007.

548  Wan, X., Kang, S., Wang, Y., Xin, J., Liu, B., Guo, Y., Wen, T., Zhang, G., and Cong, Z.: Size distribution of carbonaceous

549      aerosols at a high-altitude site on the central Tibetan Plateau (Nam Co Station, 4730ma.s.l.), Atmos. Res., 153, 155-164,

550      https://doi.org/10.1016/j.atmosres.2014.08.008, 2015.

551  Wang, M., Xu, B., Wang, N., Cao, J., Tie, X., Wang, H., Zhu, C., and Yang, W.: Two distinct patterns of seasonal variation of

552      airborne    black    carbon    over    Tibetan    Plateau,    Sci.    Total    Environ.,    573,    1041-1052,

553      https://doi.org/10.1016/j.scitotenv.2016.08.184, 2016.

554  Wiedinmyer, C., Akagi, S. K., Yokelson, R. J., Emmons, L. K., Al-Saadi, J. A., Orlando, J. J., and Soja, A. J.: The Fire

555      INventory from NCAR (FINN): a high resolution global model to estimate the emissions from open burning, Geosci.

556      Model Dev., 4, 625-641, https://doi.org/10.5194/gmd-4-625-2011, 2011.

557  Wu, G., Xu, B., Zhang, C., and Gao, S.: Atmospheric dust aerosols over the Eastern Pamirs: major element concentrations and

558      composition, Environ. Earth Sci., 61, 1227-1237, https://doi.org/10.1007/s12665-009-0446-1, 2010.

559  Xin, J. Y., Wang, Y. S., Pan, Y. P., Ji, D. S., Liu, Z. R., Wen, T. X., Wang, Y. H., Li, X. R., Sun, Y., Sun, J., Wang, P. C., Wang,

560      G. H., Wang, X. M., Cong, Z. Y., Song, T., Hu, B., Wang, L. L., Tang, G. Q., Gao, W. K., Guo, Y. H., Miao, H. Y., Tian, S.

561      L., and Wang, L.: The Campaign on Atmospheric Aerosol Research Network of China: CARE-China, Bull. Am. Meteorol.

562      Soc., 96, 1137-1155, https://doi.org/10.1175/bams-d-14-00039.1, 2015.

563  Xu, B., Wang, M., Joswiak, D. R., Cao, J., Yao, T., Wu, G., Yang, W., and Zhao, H.: Deposition of anthropogenic aerosols in a

564      southeastern Tibetan glacier, J. Geophys. Res., 114, D17209, https://doi.org/10.1029/2008JD011510, 2009.

565  Xu, C., Ma, Y. M., Panday, A., Cong, Z. Y., Yang, K., Zhu, Z. K., Wang, J. M., Amatya, P. M., and Zhao, L.: Similarities and

566      differences of aerosol optical properties between southern and northern sides of the Himalayas, Atmos. Chem. Phys., 14,

567      3133-3149, https://doi.org/10.5194/acp-14-3133-2014, 2014.

568  Xu, Y., Ramanathan, V., and Washington, W. M.: Observed high-altitude warming and snow cover retreat over Tibet and the

569      Himalayas enhanced by black carbon aerosols, Atmos. Chem. Phys., 16, 1303-1315, https://doi.org/10.5194/acp-16-1303-

570      2016, 2016.

571 Yang, J., Duan, K., Kang, S., Shi, P., and Ji, Z.: Potential feedback between aerosols and meteorological conditions in a heavy

572     pollution event over the Tibetan Plateau and Indo-Gangetic Plain, Clim. Dyn., 48, 2901-2917,

573     https://doi.org/10.1007/s00382-016-3240-2, 2017.

574 Yang, J., Kang, S., Ji, Z., and Chen, D.: Modeling the Origin of Anthropogenic Black Carbon and Its Climatic Effect Over the

575     Tibetan Plateau and Surrounding Regions, J. Geophys. Res.: Atmos., n/a-n/a, https://doi.org/10.1002/2017JD027282, 2018.

576 Yang, M., Howell, S. G., Zhuang, J., and Huebert, B. J.: Attribution of aerosol light absorption to black carbon, brown carbon,

577     and dust in China - interpretations of atmospheric measurements during EAST-AIRE, Atmos. Chem. Phys., 9, 2035-2050,

578     https://doi.org/10.5194/acp-9-2035-2009, 2009.

579 Yang, S., Xu, B., Cao, J., Zender, C. S., and Wang, M.: Climate effect of black carbon aerosol in a Tibetan Plateau glacier,

580     Atmos. Environ., 111, 71-78, https://doi.org/10.1016/j.atmosenv.2015.03.016, 2015.

581 Yao, T., Thompson, L. G., Mosbrugger, V., Zhang, F., Ma, Y., Luo, T., Xu, B., Yang, X., Joswiak, D. R., Wang, W., Joswiak,

582     M. E., Devkota, L. P., Tayal, S., Jilani, R., and Fayziev, R.: Third Pole Environment (TPE), Environ. Dev., 3, 52-64,

583     https://doi.org/10.1016/j.envdev.2012.04.002, 2012.

584 Zhang, Q., Streets, D. G., Carmichael, G. R., He, K. B., Huo, H., Kannari, A., Klimont, Z., Park, I. S., Reddy, S., Fu, J. S.,

585     Chen, D., Duan, L., Lei, Y., Wang, L. T., and Yao, Z. L.: Asian emissions in 2006 for the NASA INTEX-B mission, Atmos.

586     Chem. Phys., 9, 5131-5153, https://doi.org/10.5194/acp-9-5131-2009, 2009.

587 Zhang, R., Wang, H., Qian, Y., Rasch, P. J., Easter, R. C., Ma, P. L., Singh, B., Huang, J., and Fu, Q.: Quantifying sources,

588     transport, deposition, and radiative forcing of black carbon over the Himalayas and Tibetan Plateau, Atmos. Chem. Phys.,

589     15, 6205-6223, https://doi.org/10.5194/acp-15-6205-2015, 2015.

590 Zhang, X., Ming, J., Li, Z., Wang, F., and Zhang, G.: The online measured black carbon aerosol and source orientations in the

591     Nam Co region, Tibet, Environ. Sci. Pollut. Res., 24, 25021-25033, https://doi.org/10.1007/s11356-017-0165-1, 2017a.

592 Zhang, Y., Kang, S., Cong, Z., Schmale, J., Sprenger, M., Li, C., Yang, W., Gao, T., Sillanpää, M., Li, X., Liu, Y., Chen, P., and

593     Zhang, X.: Light-absorbing impurities enhance glacier albedo reduction in the southeastern Tibetan plateau, J. Geophys.

594     Res.: Atmos., 122, 6915-6933, https://doi.org/10.1002/2016JD026397, 2017b.

595 Zhao, S., Ming, J., Xiao, C., Sun, W., and Qin, X.: A preliminary study on measurements of black carbon in the atmosphere of

596     northwest Qilian Shan, J. Environ. Sci., 24, 152-159, https://doi.org/10.1016/s1001-0742(11)60739-0, 2012.

597 Zhu, C.-S., Cao, J.-J., Hu, T.-F., Shen, Z.-X., Tie, X.-X., Huang, H., Wang, Q.-Y., Huang, R.-J., Zhao, Z.-Z., Mocnik, G., and

598     Hansen, A. D. A.: Spectral dependence of aerosol light absorption at an urban and a remote site over the Tibetan Plateau,

599     Sci. Total Environ., 590, 14-21, https://doi.org/10.1016/j.scitotenv.2017.03.057, 2017.

600 Zou, H., Zhou, L., Ma, S., Li, P., Wang, W., Li, A., Jia, J., and Gao, D.: Local wind system in the Rongbuk Valley on the

601     northern slope of Mt. Everest, Geophys. Res. Lett., 35, L13813, https://doi.org/10.1029/2008gl033466, 2008.

602
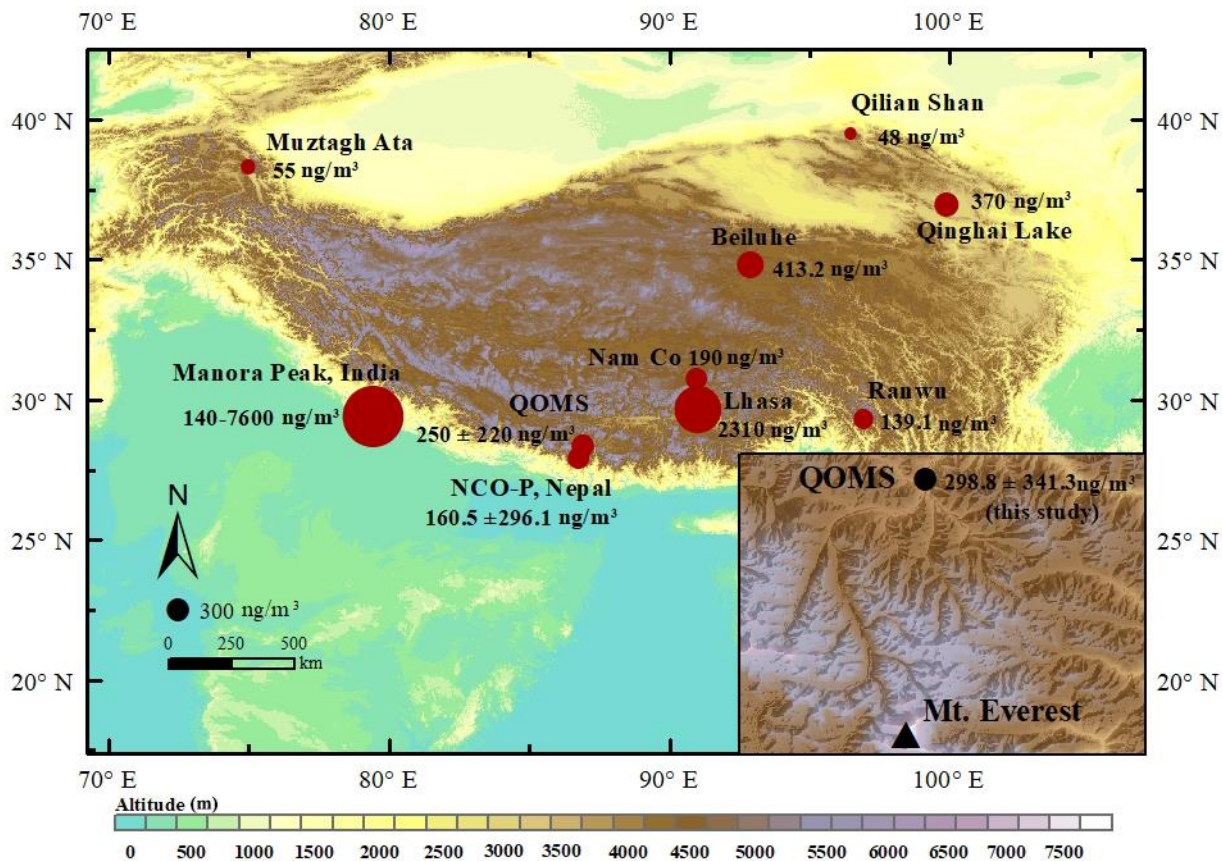
603

604 **Figure 1. Distribution of BC concentrations over the TP based on the observed values at QOMS in this study (black circle) and from**

605 **previous studies (red circles), i.e., at QOMS (Cong et al., 2015a), Nam Co (Wan et al., 2015), Lhasa (Li et al., 2016b), Ranwu (Wang**

606 **et al., 2016), Qilian Shan (Zhao et al., 2012), Beiluhe (Wang et al., 2016), Qinghai Lake (Li et al., 2013), Muztagh Ata (Cao et al.,**

607 **2009), Manora Peak, India (Ram et al., 2010), and NCO-P, Nepal (Marinoni et al., 2010).**

608

609
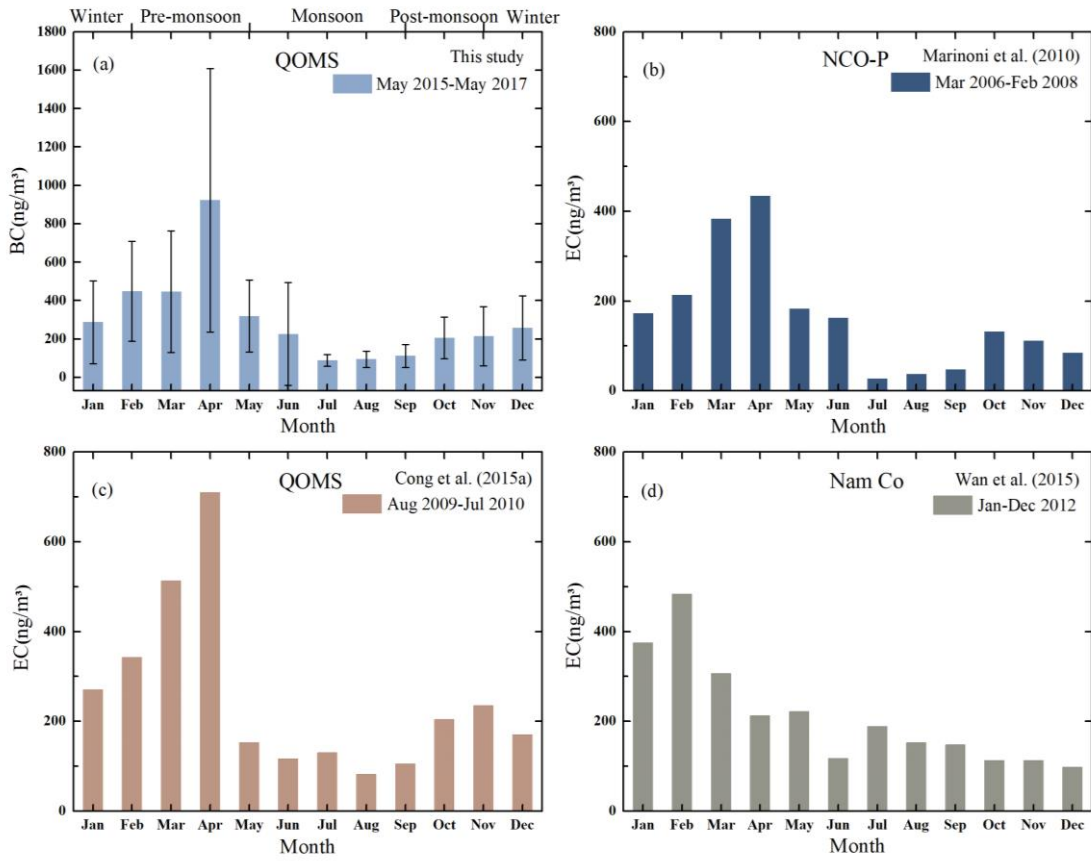
Figure 2. (a) Monthly mean BC concentrations at QOMS from May 2015 to May 2017 in this study; (b) Monthly mean EC at NCO-P from March 2006 to February 2008 from Marinoni et al. (2010); (c) Monthly mean EC at QOMS from August 2009 to July 2010 from Cong et al. (2015a); (d) Monthly mean EC at Nam Co station from January to December during 2012 from Wan et al. (2015).

613
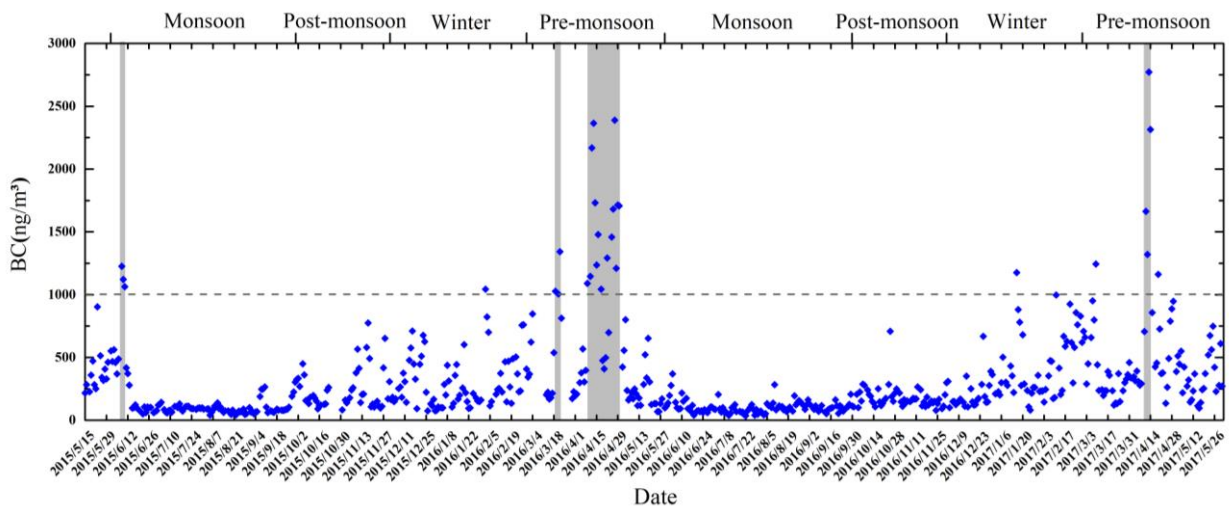
614

615 **Figure 3. Daily mean BC concentrations at QOMS during study period (the gray bars represent the continuous high values more**

616 **than 1000 ng/m³).**

617
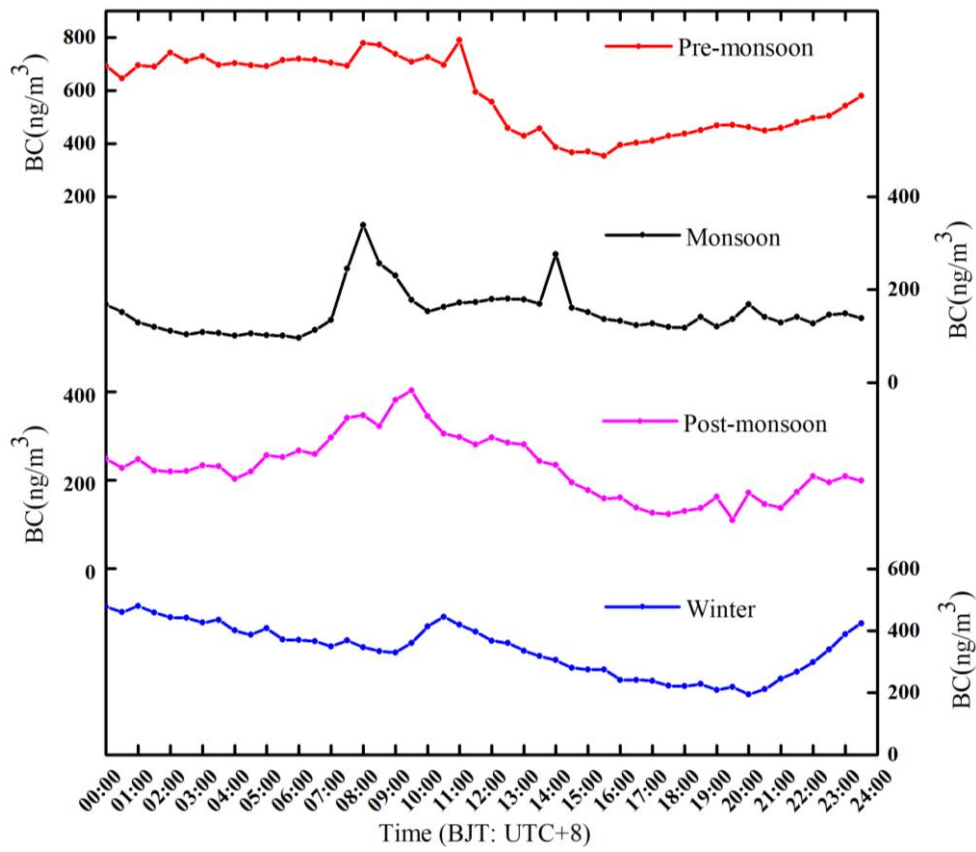
618

619 **Figure 4. Diurnal variation in BC concentrations (every half an hour) at QOMS during study period.**

620
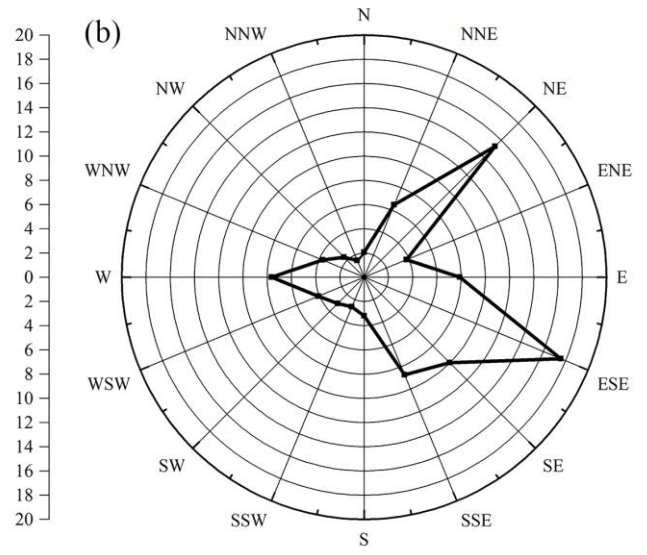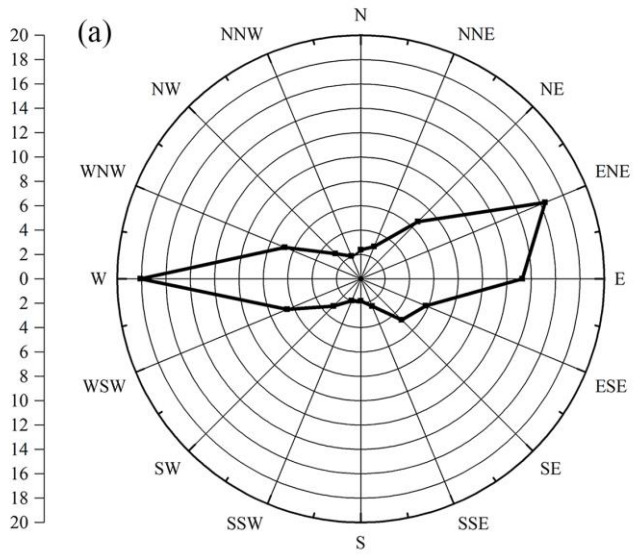
621

622    **Figure 5. Wind direction frequency at QOMS in the pre-monsoon season (a) 00:00-12:00 BJT; (b) 12:00-24:00 BJT.**

623

624
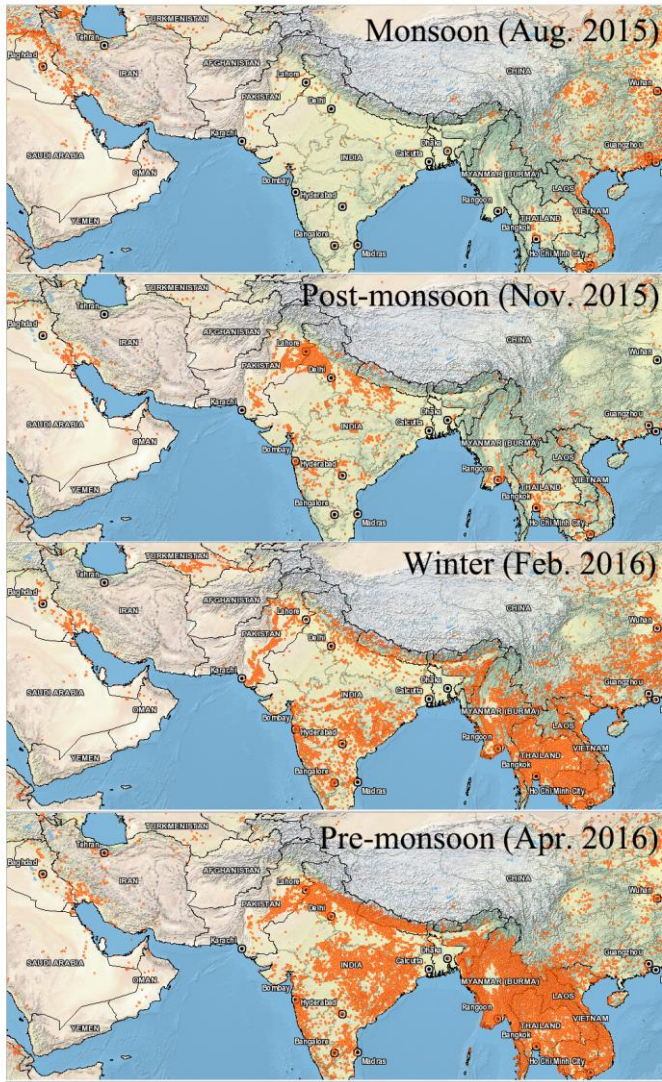
**Figure 6. Distribution of fire spots in different seasons from August 2015 to April 2016.**

626
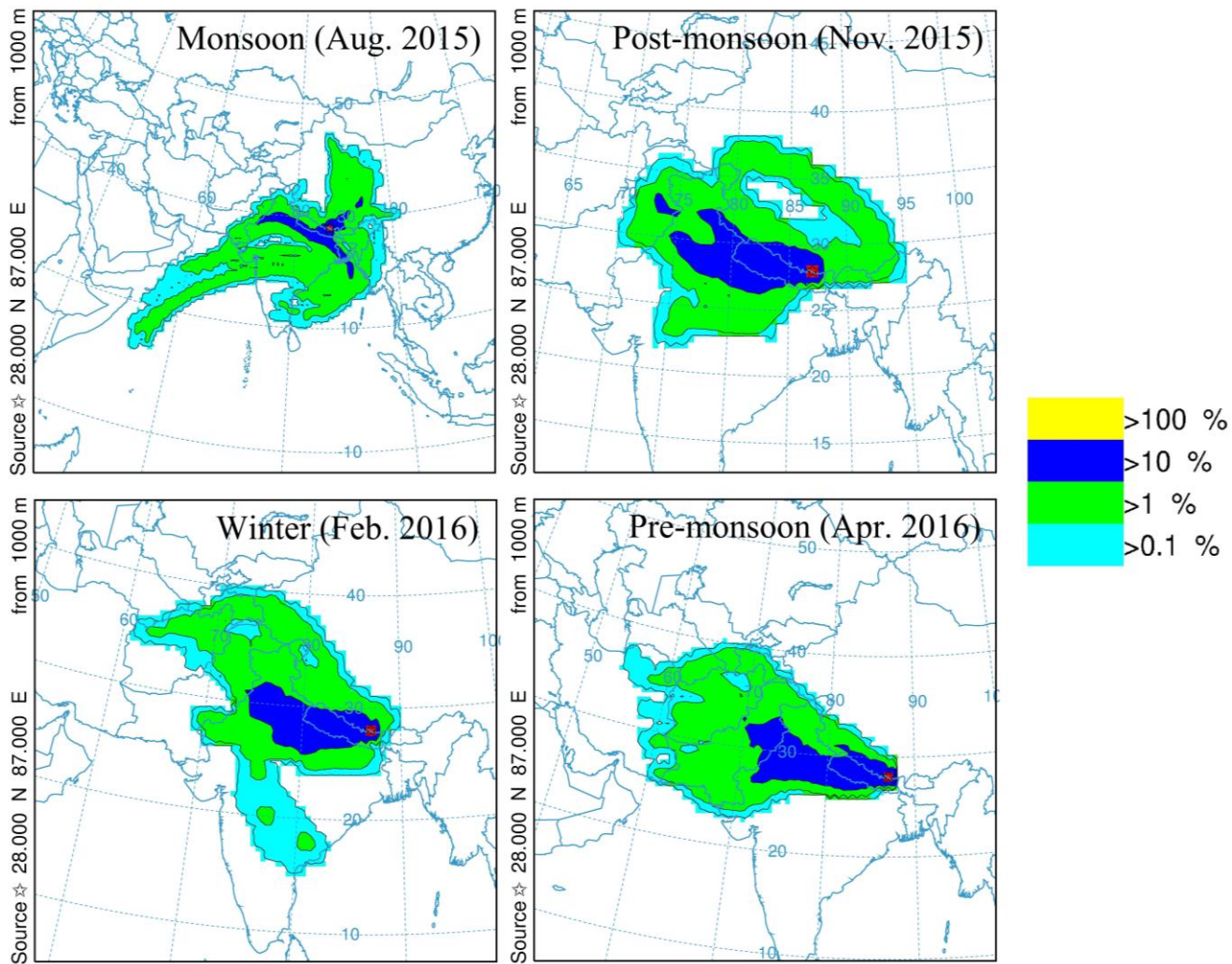
**Figure 7. Frequency plots for 5-day backward trajectories calculated by HYSPLIT model at QOMS in different seasons from August 2015 to April 2016.**

631
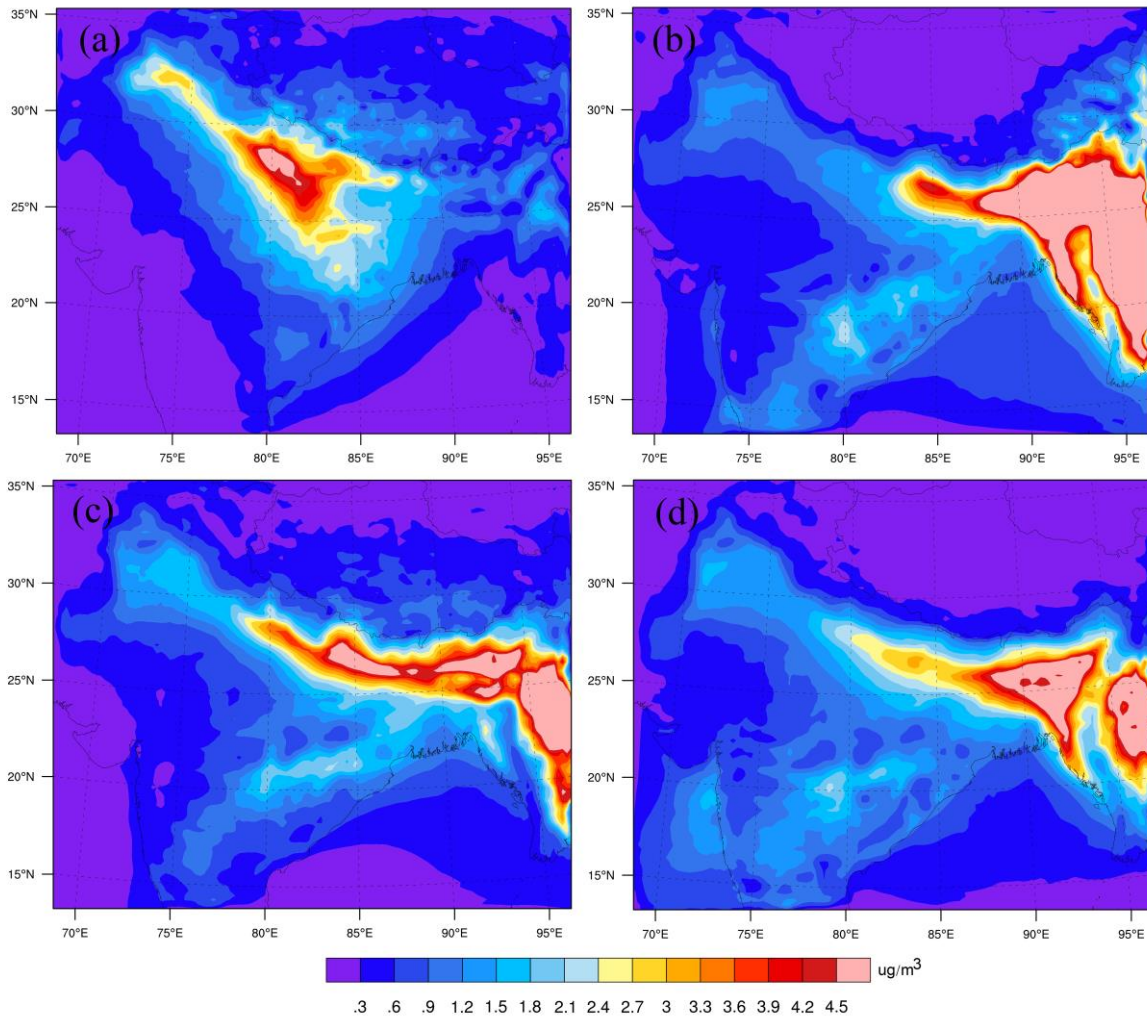
Figure 8. Mean BC concentration simulated by WRF-Chem model at QOMS and its vicinities: (a) event A; (b) event B; (c) event C; (d) event D.

632

633

634
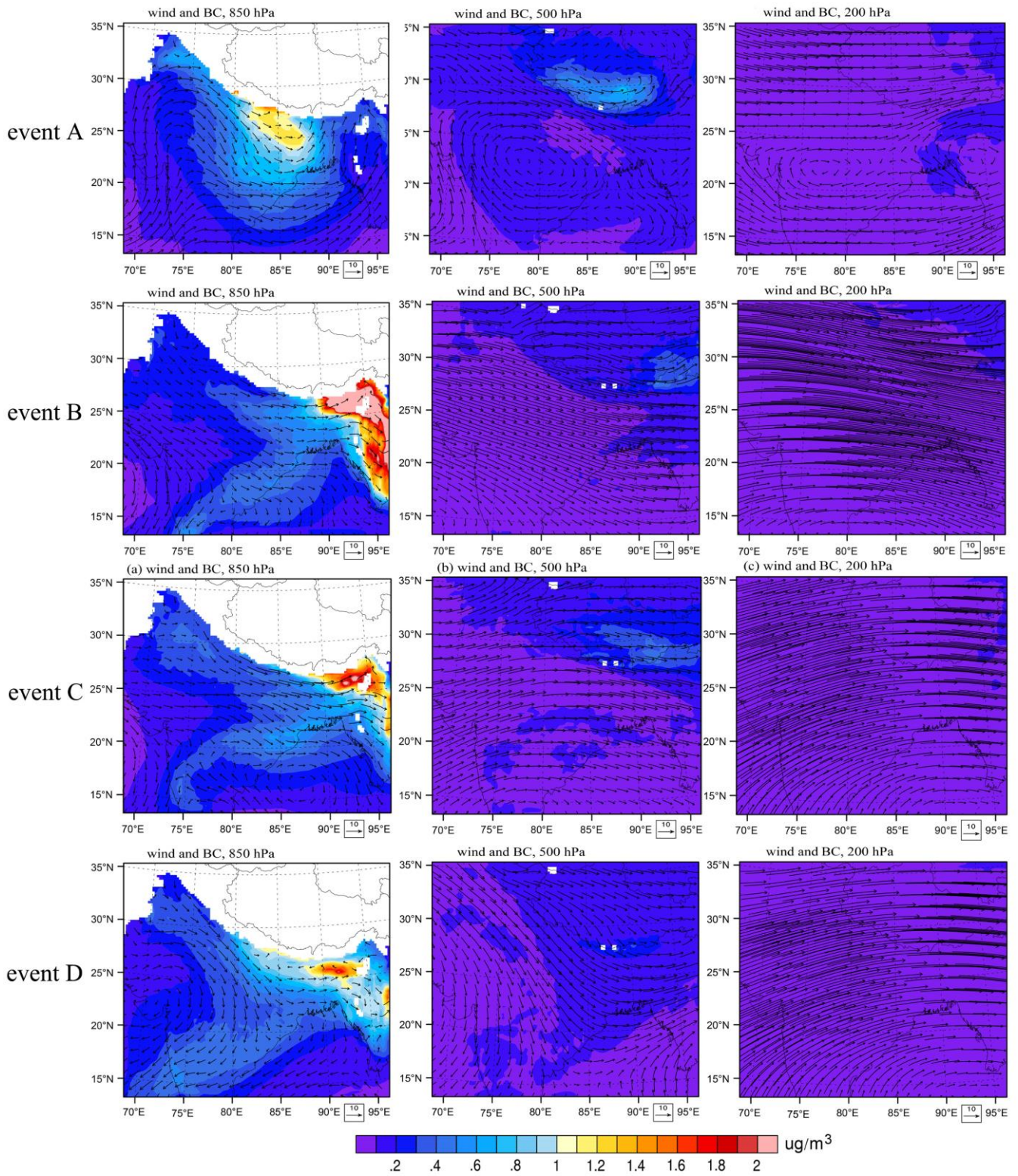
**Figure 9. Mean BC concentration and wind at 850 hPa, 500 hPa, and 200 hPa simulated by WRF-Chem model at QOMS and its**

**vicinities: event A (the first row); event B (the second row); event C (the third row); event D (the last row).**

637

638
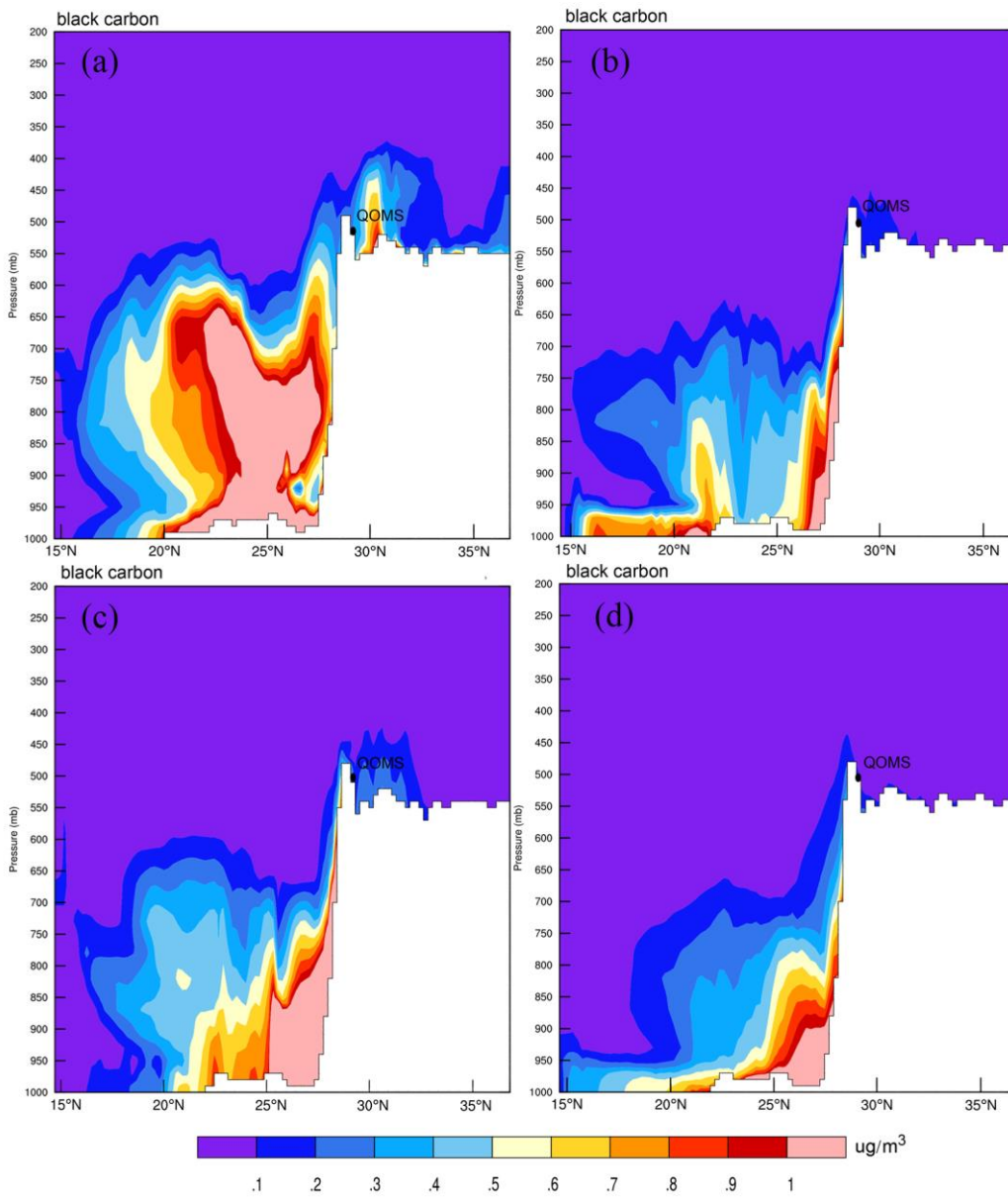
**Figure 10. Vertical profiles of mean BC concentration along the QOMS's longitude of 86.95°E: (a) event A; (b) event B; (c) event C; (d) event D.**

641

642